Chapter 2
Spin Squeezing, Entanglement and Quantum Metrology

Spin squeezing is a quantum strategy introduced in 1993 by Kitagawa and Ueda [1] which aims to redistribute the fluctuations of two conjugate spin directions among each other. In 1994 it was theoretically shown that spin squeezed states are useful quantum resources to enhance the precision of atom interferometers [2] and in 2001 the connection between spin squeezing and entanglement was pointed out [3].

In this chapter we introduce the spin representation for N two-level atoms. We review the basic theoretical concepts of spin squeezing and its connection to entanglement. Different entanglement criteria are discussed and the usefulness of entanglement as a resource in quantum metrology—focussing on spin squeezed states—is reviewed.

2.1 Collective Spins

The mathematical concept of a spin algebra with total spin J is a powerful tool to describe very different physical systems. Any observable within a spin J system can be expressed by the three spin operators $\hat{J}_x$, $\hat{J}_y$, $\hat{J}_z$ and the identity operator. The $2J + 1$ eigenstates of one of the spin operators make up a basis set of the $2J + 1$ dimensional Hilbert space. The choice of the direction is arbitrary since the operators are connected via unitary transformations.

2.1.1 A Single Spin 1/2 on the Bloch Sphere

One of the simplest nontrivial models in quantum mechanics, a two-level system [4] with levels $|a\rangle$ and $|b\rangle$, maps onto a spin $J = 1/2$ system. This mapping is done by assigning the state $|a\rangle$ to the eigenstate of $\hat{J}_z$ with eigenvalue $j_z = -1/2$ (spin down) and state $|b\rangle$ to the eigenstate with eigenvalue $j_z = +1/2$ (spin up). Two important applications of this model in atomic physics are the two-level atom and nuclear magnetic resonance experiments. Any pure quantum state

C. Groß, *Spin Squeezing and Non-linear Atom Interferometry with Bose–Einstein Condensates*, Springer Theses, DOI: 10.1007/978-3-642-25637-0_2,

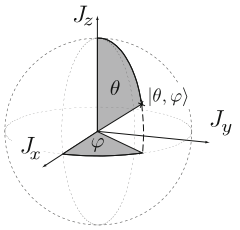

Fig. 2.1 The Bloch sphere. Schematic representation of the quantum state $|\theta, \varphi\rangle$ of a spin 1/2 system on the Bloch sphere. The definition of the longitudinal angle φ and the polar angle θ are highlighted and in the following the same notation will be used for the direction of the collective spin on a generalized Bloch sphere (see Sect. 2.2.2)

$|\theta, \varphi\rangle = \sin(\theta/2)\,|a\rangle + \cos(\theta/2)e^{i\varphi}\,|b\rangle$ of a two-level system can be conveniently represented on a *Bloch sphere*. The coordinate axes are chosen such that the population difference $(|b\rangle\langle b| - |a\rangle\langle a|)/2$ maps to the $\hat{J}_z$ component of the spin and the coherences $(|b\rangle\langle a| + |a\rangle\langle b|)/2$ and $(|b\rangle\langle a| - |a\rangle\langle b|)/2i$ map to the $\hat{J}_x$ and $\hat{J}_y$ components respectively. Figure 2.1 shows the quantum state on the Bloch sphere with the definition of the longitudinal angle φ and the polar angle θ. The Hilbert space for a single spin 1/2 system is two dimensional, such that the representation on the surface of the Bloch sphere does not require any additional assumptions.

2.1.2 A Large Collective Spin

The discussion above can be generalized for N particle systems where each particle is restricted to two modes. Each particle is an elementary spin $j = 1/2$ system, sometimes called *Qubit*.

The collective spin operators $\hat{\mathcal{J}}_i$ can be defined as the sum over all elementary spin operators (Pauli matrices) $\hat{\sigma}_i^{(k)}$, where $i = (x, y, z)$:

$$\hat{\mathcal{J}}_i = \sum_{k=1}^{N} \hat{\sigma}_i^{(k)} \tag{2.1}$$

A basis of the general problem can be obtained as the tensor product of all N bases of the individual components, each of dimension $(2j + 1)$. The dimension of the Hilbert space is huge $\dim(\mathcal{H}_\mathcal{N}) = (2j + 1)^N = 2^N$ and grows exponentially with the number of Qubits. The length of the collective spin $\mathcal{J}$ is smaller or equal than half the number of Qubits[1]:

$$\sqrt{\mathcal{J}(\mathcal{J}+1)} = \langle \hat{\mathcal{J}}^2 \rangle^{1/2} \leq N/2 \tag{2.2}$$

One often assumed simplification is exchange symmetry among all Qubits. This is physically motivated since in many experiments all operations done on the ensemble

[1] In this thesis we deal with large spins such that we often approximate $\sqrt{\mathcal{J}(\mathcal{J}+1)} \approx \mathcal{J}$.

affect each spin in the same way. One example are nuclear magnetic resonance experiments in homogeneous fields.

In the symmetric case each elementary Qubit can be prepared for example in the $j_z = -1/2$ state and maximum collective polarization $J_z = -N/2$ can always be reached. Therefore the total spin length is given by $J = N/2$ and the dimension of the Hilbert space dramatically reduces to $\dim(\mathcal{H}_S) = (2Nj + 1) = (N + 1)$, linearly dependent on the number of Qubits. One possible choice of a basis are the symmetric *Dicke states* $|J, m\rangle$ with $-N/2 < m < N/2$. Due to their exchange symmetry the elementary spins can be effectively described as Bosons, the *Schwinger Bosons* [5]. Employing the second quantization formalism the creation and annihilation operators of the two modes $\hat{a}^\dagger$ ($\hat{b}^\dagger$) and $\hat{a}$ ($\hat{b}$) can be related to the different spin components [6]:

$$\begin{aligned}
\hat{J}_+ &= \hat{b}^\dagger \hat{a} \\
\hat{J}_- &= \hat{a}^\dagger \hat{b} \\
\hat{J}_x &= \frac{1}{2}(\hat{J}_+ + \hat{J}_-) \\
\hat{J}_y &= \frac{1}{2i}(\hat{J}_+ - \hat{J}_-) \\
\hat{J}_z &= \frac{1}{2}(\hat{b}^\dagger \hat{b} - \hat{a}^\dagger \hat{a})
\end{aligned}$$

Each of the Dicke states introduced above corresponds to a perfectly defined particle number difference between the two modes $\hat{a}$ and $\hat{b}$ and since the total number of particles N is fixed the Dicke states correspond to *Fock states* in the two modes $\hat{a}$ and $\hat{b}$.

The experiments presented in this thesis deal with two-mode Bose–Einstein condensates. Identical particles in two modes (as the Bosons in the condensate) can be described by the symmetric spin model and the *Schwinger representation* given above is used to relate the creation and annihilation operators of the two modes to the different spin components.

Even if not formally correct we will use the notation J instead of $\mathcal{J}$ for all spins regardless of symmetry and mention explicitly where the symmetry argument is necessary.

2.2 Fluctuation Engineering

The three different orthogonal spin components are conjugate variables. Their commutation relation is $[\hat{J}_i, \hat{J}_j] = i\epsilon_{ijk}\hat{J}_k$, where ϵ_{ijk} is the Levi-Civita symbol. Therefore any pair of spin operators obeys a Heisenberg uncertainty relation which—for $\Delta\hat{J}_z^2$ and $\Delta\hat{J}_y^2$—is given by

$$\Delta \hat{J}_z^2 \Delta \hat{J}_y^2 \geq \frac{1}{4} \langle \hat{J}_x \rangle^2 \tag{2.3}$$

and $\Delta \hat{J}_z^2 = \langle \hat{J}_z \rangle^2 - \langle \hat{J}_z \rangle^2$ is the variance in $\hat{J}_z$ direction.

2.2.1 Coherent Spin States

Coherent spin states are the most classical-like pure quantum states of a symmetric ensemble of N elementary $j = 1/2$ spins or of N two-mode Bosons [6, 7]. They are constructed by placing all N particles in the same single particle state in any superposition of the two modes

$$|\theta, \varphi\rangle = \frac{1}{\sqrt{N!}} [\sin(\theta/2)\hat{a}^\dagger + \cos(\theta/2) e^{i\varphi} \hat{b}^\dagger]^N |\text{vac}\rangle \tag{2.4}$$

where $|\text{vac}\rangle$ is the vacuum state. Especially no quantum correlations between the particles are present. Therefore a coherent spin state features equal variance in any direction $\hat{J}_\perp$ orthogonal to the mean spin direction (θ, φ) which is given by the sum of the variances of the $2J$ elementary spin 1/2 particles. The perpendicular variances $\Delta \hat{\sigma}_\perp^2$ of individual Qubits are by definition isotropic around (θ, φ) since there are no subsystems that could cause any correlations [1]. The Heisenberg limit (2.2) for a single elementary spin pointing in σ_x direction is $\Delta \sigma_z^2 \Delta \sigma_y^2 = \frac{1}{4} \cdot \frac{1}{4}$ leading to an isotropic variance of

$$\Delta \hat{J}_z^2 = \Delta \hat{J}_y^2 = 2J \cdot \frac{1}{4} = \frac{J}{2} \tag{2.5}$$

for the collective coherent spin state, which identifies this quantum state as a minimal uncertainty state since $\langle \hat{J}_x \rangle = J$. We refer to the perpendicular spin fluctuations of a coherent spin state $\Delta \hat{J}_\perp^2 = J/2 = N/4$ as the *shot noise limit*.

We go back to the first quantization formalism in order to obtain the probability distribution over different sets of basis states—especially the two possible Dicke state bases in the directions orthogonal to the mean spin direction. In order to develop a more detailed understanding of the coherent spin state and its fluctuations we start with the discussion of a special case where each particle is in a 50/50 superposition of the two modes with 0 relative phase—each spin points in σ_x direction and its quantum state is

$$|x\rangle = \left(\left| \frac{1}{2}, -\frac{1}{2} \right\rangle + \left| \frac{1}{2}, +\frac{1}{2} \right\rangle \right) / \sqrt{2} \tag{2.6}$$

where we have chosen the Dicke states in σ_z direction as the basis states. The probability to observe each individual elementary spin in state up or down is equal

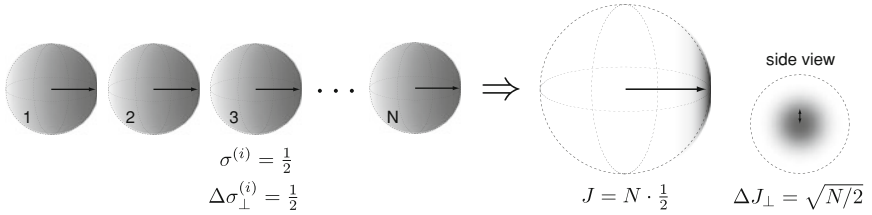

Fig. 2.2 A coherent spin state composed of elementary spins. The figure illustrates the addition of N elementary Qubits with equal mean spin orientation (*indicated by the arrows*) to a large collective spin J . The gray shading on the Bloch spheres visualizes the spread of the quantum state on the sphere using the Q-representation introduced in Sect. 2.2.2. The isotropic angular uncertainty decreases with the number of Qubits according to the standard quantum limit

$\left|\langle\frac{1}{2}, \pm\frac{1}{2}|x\rangle\right|^2 = 1/2$. The N atom coherent spin state is a collection of these independent elementary spins

$$|X\rangle = \left[\left(\left|\frac{1}{2}, -\frac{1}{2}\right\rangle + \left|\frac{1}{2}, +\frac{1}{2}\right\rangle\right)/\sqrt{2}\right]^{\otimes N} \tag{2.7}$$

and therefore the measurement of the J_z spin component is equivalent to N measurements on a single spin and the probability distribution over the Dicke states is binomial. We could have chosen equally the Dicke states in J_y direction to describe the spin state which shows again that the spin fluctuations in the directions perpendicular to J_x—the mean spin direction—are isotropic.

A general coherent spin state $|\theta, \varphi\rangle$ described as superposition of Dicke states $|J, m\rangle$ is given by [8]:

$$|\theta, \varphi\rangle = \sum_{m=-J}^{J} c_m(\theta) \mathrm{e}^{-i(J+m)\varphi} |J, m\rangle \tag{2.8}$$

As argued above the coefficients $c_m(\theta)$ follow a binomial distribution peaked around θ:

$$c_m(\theta) = \binom{2J}{J+m}^{1/2} \cos(\theta/2)^{J-m} \sin(\theta/2)^{J+m} \tag{2.9}$$

Figure 2.2 depicts the composition of a large collective spin from elementary spins on generalized Bloch spheres.[2] The illustration of the spins is done using the Q-representation described in Sect. 2.2.2.

The Standard Quantum Limit

Due to the Heisenberg uncertainty principle (2.2) the mean direction (θ, φ) of any spin state can not be defined with arbitrary precision. For a coherent spin state the

[2] Above we give an example for the mean spin in J_x direction, however for the purpose of better illustration we have chosen a different direction in the figure.

isotropic angular uncertainty $\Delta\varphi = \Delta\theta$, defined by the ratio of the uncertainty of the perpendicular spin directions $\Delta J_\perp$ to the mean spin length J, is given by:

$$\Delta\varphi = \frac{\Delta\hat{J}_\perp}{\langle\hat{J}\rangle} = \frac{1}{\sqrt{2J}} = \frac{1}{\sqrt{N}} \tag{2.10}$$

As argued above this limit arises as the classical statistical limit in a system consisting of N independent constituents [2, 9]. In Sect. 2.4 we discuss the connection of spin states and Ramsey interferometry and we show that the angular uncertainty limits the interferometric precision. In this context the "classical" limit (2.10) for a coherent spin state is known as the *standard quantum limit*. Figure 2.2 also visualizes the decreasing angular uncertainty with the number of elementary spins.

2.2.2 Visualizing Spin States: The Husimi Q-Representation

Employing the Q-representation [10], spin states can be conveniently visualized on a generalized Bloch sphere with radius J. In order to describe the most general spin state, i.e. pure states and statistical mixtures, the density matrix formalism is used [6]. The density operator $\hat{\rho}$ in coherent spin state basis is given by

$$\hat{\rho} = \int P(\theta,\varphi)|\theta,\varphi\rangle\langle\theta,\varphi|\mathrm{d}\Omega \tag{2.11}$$

where the integral covers the full solid angle and $\mathrm{d}\Omega = \sin(\theta)\mathrm{d}\theta\mathrm{d}\phi$. The probability distribution $P(\theta,\varphi)$ is normalized to one. The Q-representation uses the diagonal elements of the density operator to represent the quantum state:

$$Q(\theta,\varphi) = \frac{2J+1}{4\pi}\langle\theta,\varphi|\rho|\theta,\varphi\rangle \tag{2.12}$$

The interpretation of this representation on generalized Bloch spheres differs from the single spin $j = 1/2$ Bloch sphere shown in Fig. 2.1. In the latter case the dimension of the Hilbert space is two-dimensional and the quantum state representation on the surface of a sphere is exact. However for collective spin systems the dimension of the Hilbert space is $2J + 1$ such that an exact mapping to the surface of a sphere is not possible. The position (θ, ϕ) on the spin 1/2 Bloch sphere describes the full quantum state, while the position on the generalized Bloch sphere gives only the mean spin direction and—within the constraints explained below—its fluctuations. The Q-representation projects the density matrix on minimal uncertainty states, in particular coherent spin states. The most obvious consequence is that the minimal extension of a quantum state in (θ, φ) on the Bloch sphere is given by the uncertainties of the basis states—a single Dicke state features no uncertainty in polar direction but its Q-representation shows $\Delta\theta \propto 1/\sqrt{N}$.

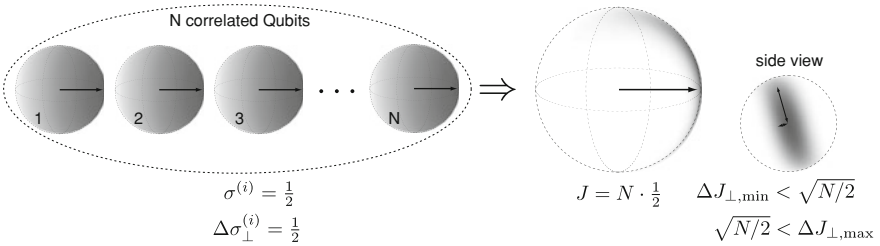

Fig. 2.3 Spin squeezed states. The figure illustrates an exemplary pure spin squeezed state on the Bloch sphere. The individual Qubits feature an isotropic variance, but quantum correlations between them cause an anisotropic variance of the collective spin state. For a Heisenberg limited spin squeezed state, one of the perpendicular variances $\Delta J_{\perp,\min}$ is smaller than the variance of a coherent spin state (of the same spin length), while the variance in the second perpendicular direction $\Delta J_{\perp,\max}$ is increased

2.2.3 Spin Squeezed States

Quantum correlations between the elementary spin 1/2 particles of a collective spin J can cause anisotropic fluctuations of the spin vector in the directions perpendicular to the mean spin (Fig. 2.3). Nevertheless the fluctuations of each individual elementary spin are always isotropic [1]. In Ref. [1] quantum states are considered spin squeezed if the variance of one spin component is smaller than the shot noise limit $J/2$ for a coherent spin state:

$$\xi_N^2 = \frac{2}{J}\Delta\hat{J}_{\perp,\min}^2 \tag{2.13}$$

Definition (2.13) does not take the second perpendicular spin direction into account. Due to the Heisenberg uncertainty relation (2.2) reduction of the variance in one direction causes an increase of fluctuations in the other. Real life strategies to obtain spin squeezing might also involve states that are not minimal uncertainty states. One example is the “one axis twisting" scheme proposed in [1], which we use in the experiments described in the last chapter of this thesis. For these states, as for experimentally very important non-pure quantum states, the variance in some other direction than the squeezed direction can be much larger than given by the Heisenberg uncertainty relation. This leads to a reduction of the effective mean spin length $\langle\hat{\mathbf{J}}\rangle$.

Metrologic applications, especially Ramsey interferometry for which spin squeezed states have been considered useful, require a large mean spin length. In order to measure the usefulness of spin squeezed states for these applications another definition of the squeezing parameter was introduced in Ref. [2]

$$\xi_R = \sqrt{2J}\frac{\Delta\hat{J}_{\perp,\min}}{\langle\hat{\mathbf{J}}\rangle} \tag{2.14}$$

whose inverse ξ_R^{-1} measures the precision gain in a Ramsey interferometric sequence relative to the standard quantum limit (2.10). For a detailed discussion of interferometry with spin squeezed states see Sect. 2.4

Spin squeezing among N constituents is related to *many-body entanglement*. In this context a third spin squeezing criterion was found [3]:

$$\xi_S^2 = N \frac{\Delta \hat{J}^2_{\perp,\min}}{\langle \hat{\mathbf{J}} \rangle^2} = N \frac{\Delta \hat{J}_z^2}{\langle \hat{J}_x \rangle^2} \tag{2.15}$$

Entanglement is detected by the inequality $\xi_S^2 < 1$ as detailed in the following section. Here we explicitly use the standard assumption throughout this thesis that the mean spin points in J_x direction and the direction of minimal variance—if not explicitly mentioned—is the J_z direction.

ξ_S can be used equivalently to ξ_R to quantify spin squeezing and precision gain in interferometry and we refer to it as *coherent number squeezing* or *coherent spin squeezing*.

2.3 Spin Squeezing and Entanglement

2.3.1 Definition of Many-Body Entanglement

For N distinguishable particles the definition of a separable state, i.e. non-entangled state, is that its N-body density matrix ρ can be written as a direct product of single particle density matrices $\rho^{(i)}$:

$$\rho = \sum_k p_k \rho_k^{(1)} \otimes \rho_k^{(2)} \otimes \cdots \otimes \rho_k^{(N)} \tag{2.16}$$

p_k is a probability distribution to account for incoherent mixtures. Entanglement in many-body systems (for a general review see [11, 12]) is defined as the non-separability of the density matrix ρ meaning the equality in Eq. 2.16 does not hold.

In collective spin systems a separable state is composed of independent elementary spin 1/2 particles. Due to technical limitations the individual elementary spins can not be addressed in many experiments . However it is important to note that the elementary spins have to be in principle distinguishable in order to define entanglement among them in a meaningful way [11]. In the scope of this thesis we deal with N particles in a Bose–Einstein condensate where the distinguishability is not obvious. However Sørensen and Mølmer pointed out that by a gedanken local operation one can pinpoint each particle in space without affecting the spin properties of the system (Sørensen AS, Mølmer K private communication). The distinguishability is now given via the position of each particle. If entanglement is detected in the system, it must have been present in the system before the localization, since local measurements can not generate entanglement [13]. Given that the atoms in the Bose–Einstein

condensate are spaced by more than one wavelength of the detection light (which is usually fulfilled), this gedanken local operation means to overcome the technical limitations for addressability and detection of the individual Qubits.

The question of entanglement in bosonic pseudo spin systems and its connection to spin squcezing are extensively discussed in [14].

2.3.2 Entanglement Criteria Based on Collective Spin Variables

Without the possibility to address the individual Qubits entanglement criteria based on the collective spin variables are necessary to detect entanglement. Furthermore the observables in most experiments so far are limited to first and second order moments of the distributions functions in different spin directions due to rather small counting statistics and technical noise. Based on these, a complete set of inequalities that is fulfilled for any separable quantum state has been found [15, 16]. Complete in this sense means that assuming the only information available are first ($\langle \hat{J}_x \rangle, \langle \hat{J}_y \rangle, \langle \hat{J}_z \rangle$) and second moments ($\Delta \hat{J}_x^2, \Delta \hat{J}_y^2, \Delta \hat{J}_z^2$) of the distribution functions. These inequalities are:

$$\langle \hat{J}_x^2 \rangle + \langle \hat{J}_y^2 \rangle + \langle \hat{J}_z^2 \rangle \leq \frac{N(N+2)}{4} \tag{2.17}$$

$$\Delta \hat{J}_x^2 + \Delta \hat{J}_y^2 + \Delta \hat{J}_z^2 \geq \frac{N}{2} \tag{2.18}$$

$$\langle \hat{J}_i^2 \rangle + \langle \hat{J}_j^2 \rangle - \frac{N}{2} \leq (N-1) \Delta \hat{J}_k^2 \tag{2.19}$$

$$(N-1)[\Delta \hat{J}_i^2 + \Delta \hat{J}_j^2] \geq \langle \hat{J}_k^2 \rangle + \frac{N(N-2)}{4} \tag{2.20}$$

Toth et al. published these inequalities in Refs. [15, 16] and the authors depict the inequalities by a volume containing all separable states in a three dimensional space spanned by ($\Delta \hat{J}_x^2, \Delta \hat{J}_y^2, \Delta \hat{J}_z^2$).

Throughout this thesis we use the original spin squeezing inequality (2.15) in order to detect spin squeezing type entanglement experimentally [3]. All separable states fulfill the inequality $\xi_S^2 \geq 1$, but a subgroup of entangled states violate it.

As pointed out in Ref. [16], this criterion is equivalent to criterion (2.20) in the limit of large N and the mean spin pointing in J_x direction.

None of the entanglement witnesses given in this section requires any symmetry assumption. They are valid for the general definition of the collective spin given in Eq. 2.1. Entanglement criteria only valid under the symmetric two-mode assumption are discussed in the next section.

Entanglement Criteria for Symmetric States

Making the strong assumption of symmetry under particle exchange many entanglement criteria simplify. In this case the detection of spin fluctuations in one direction below the shot noise limit for N atoms implies entanglement [17–20].

$$\xi_N^2 = \frac{4\Delta \hat{J}_{\perp,\min}^2}{N} = \frac{2\Delta \hat{J}_{\perp,\min}^2}{J} \geq 1 \tag{2.21}$$

holds for any separable symmetric state. For clarity the mean spin is assumed to point in J_x direction such that $\langle \hat{J}_{\perp,\min} \rangle = 0$.[3] Equation (2.21) is identical to the spin squeezing definition of Kitagawa and Ueda (2.13) showing that at least in the symmetric two-mode case entanglement is necessary to redistribute the fluctuations of orthogonal spin components. Within this thesis we refer to ξ_N^2 as *number squeezing*.

All entanglement witnesses discussed here are based on second moments, therefore they contain maximally two body correlations $\langle \hat{\sigma}_k^{(i)} \hat{\sigma}_k^{(j)} \rangle$ of the elementary spins i and J in direction k. The question arises if these criteria detect only *bipartite entanglement*, the non-separability of the average two-body density matrix.

Toth, et al. show in Ref. [16] that in the non-symmetric case the complete set of separability criteria (Eqs. 2.17–2.20) can detect entanglement even if there is no bipartite entanglement in the system—the average two-body density matrix of an non-symmetric state can be separable even if the N-body density matrix is entangled. The situation is different in the symmetric case. Here the violation of the number squeezing criterion (2.21) is both necessary and sufficient for bipartite entanglement in the system. Every bipartite entangled symmetric state features number squeezing [17].

2.3.3 Experimentally Used Quantification of Entanglement

The criteria given above are useful to detect the presence of entanglement, however they do not quantify entanglement in the system.[4] Two experimentally used approaches to quantify entanglement are reviewed here.

Von Neumann Entropy

In a recent experiment entanglement has been reported based on the *von Neumann entropy* [21]. However, we clarify in this short section that it is not possible to characterize entanglement in our experimental system by this measure.

For *pure* quantum states the von Neumann entropy $S_N(\hat{\rho}_A) = -\mathrm{Tr}(\hat{\rho}_A \log(\hat{\rho}_A))$ of the reduced density matrix $\hat{\rho}_A = \mathrm{Tr}_B(\hat{\rho})$ is a measure for *bipartite* entanglement [11, 13, 22] between one subsystem $\hat{\rho}_A$ and the rest of the system $\hat{\rho}_B = \mathrm{Tr}_A(\hat{\rho})$. There is

[3] The general expression is $\frac{4\Delta \hat{J}_k^2}{N} \geq 1 - \frac{4\langle \hat{J}_k \rangle^2}{N^2}$ [19].

[4] Since criterion (2.15) can be related to a gain in interferometric precision (see Sect. 2.4), it measures the "usefulness" of spin squeezed states as a quantum resource in a known experimental protocol.

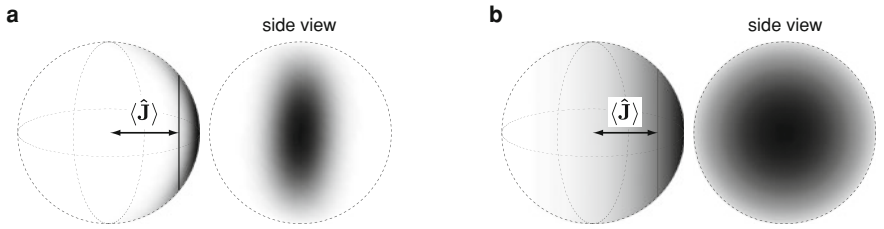

Fig. 2.4 Von Neumann entropy and delocalization of the quantum state. Panel **a** depicts an entangled spin squeezed state on the Bloch sphere. Quantum correlations cause an increased uncertainty in one spin direction which results in a shortening of the effective spin length. This shortening is measured by the linearized von Neumann entropy. Panel **b** shows a non-entangled incoherent mixture. Loss of coherence results also in a shortening of the mean spin length, making it hard to use the von Neumann entropy for our experiments where temperature or environmental noise cause decoherence

no difference on which of the two subsystem S_N is evaluated: $S_N(\hat{\rho}_A) = S_N(\hat{\rho}_B)$. Expanding the von Neumann entropy to first order one obtains the linear entropy:

$$S_N = 1 - \mathrm{Tr}(\hat{\rho}_A^2) \tag{2.22}$$

Taking subsystem A to be a single elementary spin 1/2 particle, S_N can be used to measure entanglement between one Qubit and the rest of the system. The density matrix $\hat{\rho}_A$ can be expressed as a linear combination of Pauli matrices σ_i [23]. If the system is additionally in a symmetric state, the linearized von Neumann entropy can be related to the mean values of the collective spin J [21, 24]:

$$S_N = \frac{1}{2}[1 - \frac{4}{N^2}(\langle \hat{J}_x \rangle^2 + \langle \hat{J}_y \rangle^2 + \langle \hat{J}_z \rangle^2)] \tag{2.23}$$

Figure 2.4 illustrates the linear entropy measure and clarifies its connection to the spread of the state on the Bloch sphere. Since mixed states always have an (incoherently) increased spread it is essential to note its applicability to pure states only. The quantum states realized in our experiments are subject to decoherence making it impossible to apply the linear entropy measure.

Depth of Entanglement

In the context of spin squeezing the *depth of entanglement* has been proposed to quantify entanglement [25] which measures the number of non-separable elementary Qubits. This criterion is valid for incoherent mixtures as well as for pure states making it suitable for our experiments. However, we once again emphasize that there is no clear definition for entanglement among indistinguishable particles. Furthermore, unique entanglement measures for more than two or three particles are still a very active field of research [11].

We review the depth of entanglement criterion here and use the label J for the collective spin of the full system and the label S for subsystems of smaller spin, but

not necessarily $S = 1/2$. The basic idea is to find the minimal variance $\Delta\hat{S}_z^2$ for a given mean spin length $\langle\hat{S}_x\rangle$. Combining the inequality $\langle\hat{S}_z^2\rangle+\langle\hat{S}_y^2\rangle+\langle\hat{S}_z^2\rangle \leq S(S+1)$ (which is similar to Eq. 2.17) with the Heisenberg uncertainty limit (2.2) one obtains

$$\Delta\hat{S}_z^2 \geq \frac{1}{2}\left[S(S+1) - \langle\hat{S}_x\rangle^2 - \sqrt{(S(S+1) - \langle\hat{S}_x\rangle^2)^2 - \langle\hat{S}_x\rangle^2}\right] \tag{2.24}$$

as an analytical estimation of the limit.

Numerical calculations allow to set the bound even tighter [25] and a comparison between the numerical results and the analytical formula is shown in Fig. 2.5. From Fig. 2.5 it is obvious that large spins S can be more squeezed than small spins.[5] This implies that a collective spin J composed of k subsystems with spin $S^{(k)}$ can be more squeezed than the individual spins $S^{(k)}$. In other words, one perfectly squeezed large spin J has always lower or equal normalized variance $\Delta\hat{J}_z^2/J$ for a given normalized mean spin length $\langle\hat{J}_x\rangle/J$ than the sum of the normalized variances of N independent but individually perfectly squeezed smaller spins $S^{(k)}$ for the same normalized mean spin length. Based on these findings the authors of Ref. [25] derive a lower bound for the variance of the collective spin $\Delta\hat{J}_z^2$

$$\Delta\hat{J}_z^2/NS \geq F_S(\langle\hat{J}_z\rangle/NS) \tag{2.25}$$

where $F_S(.)$ is the minimum for spin S shown in Fig. 2.5.

The interpretation of this result in the case of N spin 1/2 particles is: If one measures the pair $\Delta\hat{J}_z^2/J$ and $\langle\hat{J}_x\rangle/J$ outside the gray shaded area in Fig. 2.5, entanglement has to be present in the system. Depending on which curve m the measured datapoint falls, the minimal size of the largest non-separable spin has to be $S = m \cdot 1/2$ and the number of these non-separable blocks is N/m.

What happens if N/m is not an integer value? In this case there has to be one or more smaller blocks of entangled (or even non-entangled) particles, causing larger fluctuations than in the case of exactly N/m particles with spin $S = m \cdot 1/2$ since smaller spins cause larger fluctuations. In order to explain the observed data point, the largest entangled block has to be even greater than m. To summarize, minimally m entangled Qubits are detected if the measured datapoint falls on the curve for $S = m \cdot 1/2$.

2.4 Entangled Interferometry

Entanglement in collective spin systems is not only interesting from a conceptual perspective but it has also been shown to provide a useful quantum resource. In 1994 Wineland et al. [2] pointed out, that in particular spin squeezed states can be used to overcome the standard quantum limit in metrology.

[5] As already mentioned a spin $S = 1/2$ can not be squeezed at all.

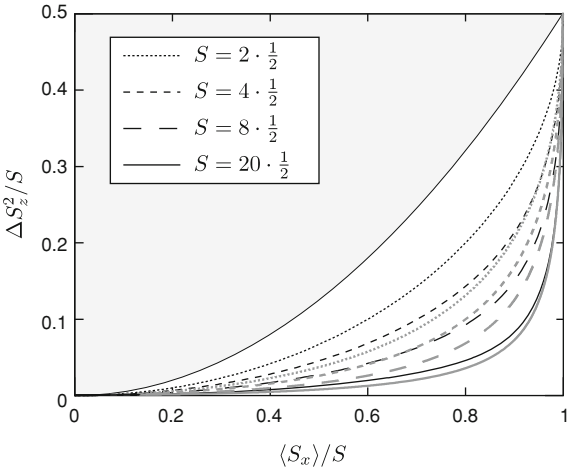

Fig. 2.5 Depth of entanglement. The figure shows the minimal allowed normalized variance $\Delta \hat{S}_z^2$ for a given mean spin length $\langle \hat{S}_x \rangle$ depending on the total spin S (different line styles). The black lines are the numerical result taken from reference [25] (Fig. 2.1) while the gray lines show the analytic approximation (2.24) which we use later in this thesis. The spin length S is written as $S = m \cdot 1/2$ in order to emphasize the minimal non-separable block size m of the density matrix in the case of Qubits as elementary spins. The gray area correspond to pairs of $\langle \hat{S}_x \rangle / S$ and $\Delta \hat{S}_z^2 / S$ for which no entanglement is detected in the system

2.4.1 Precision Limits in Ramsey Interferometry

The term *Ramsey interferometry* [26, 27] is used most often for atomic interferometers based on internal states. Prominent applications are the definition of the time standard [28] or high precision magnetometry [29]. However the scheme is more general and applies also to atom interferometers where the two states are implemented using external degrees of freedom. These interferometers allow for example for high precision inertia measurements of gravity or rotation [30–32]. The optical counterpart of Ramsey interferometry is a Mach–Zehnder interferometer and the analogy is further discussed in Sect. 4.7 .

The Ramsey Interferometric Sequence

In order to develop an intuitive understanding for the precision limit in interferometry we discuss the implementation of a typical Ramsey interferometer and visualize the protocol schematically on Bloch spheres (Fig. 2.6a). A Ramsey atom interferometer conceptually consists of at least three building blocks, two beamsplitters and an evolution time in between. The first beamsplitter, which corresponds to a unitary rotation on the Bloch sphere around an axis in the equatorial plane, is used to generate a coherent superposition of the two quantum states. Assuming only one input port to be populated the output is usually a collective spin state with the mean spin pointing onto the equator. A fixed time τ of free evolution follows during which a relative

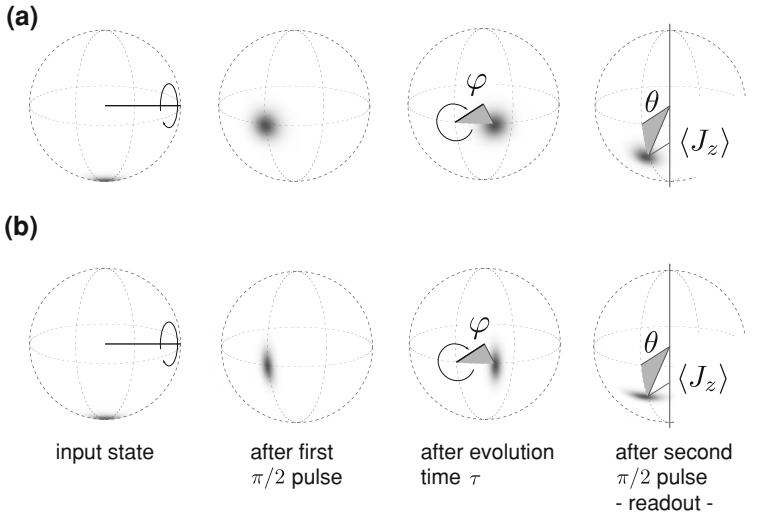

Fig. 2.6 Schematic representation of Ramsey interferometry on the Bloch sphere. Part **a** shows the standard Ramsey protocol represented on the Bloch sphere. Beamsplitters correspond to rotations of the quantum state around an axis in the equatorial plane as indicated by the circular shaped arrows. The sequence is described in detail in the main text. Panel **b** shows a similar protocol but after the first "magic" beamsplitter a spin squeezed state emerges which propagates through the interferometer resulting in degreased occupation number uncertainty at the readout. Section 4.7 of this thesis describes the concrete implementation of this "magic"—non-linear—beamsplitter

phase φ between the two modes accumulates (corresponding to a longitudinal rotation on the Bloch sphere). Depending on the kind of interferometer this phase is due to differential energy shifts between the states or due to effective path length differences to be measured [30]. Since the angle in longitudinal direction on the Bloch sphere φ is usually not directly observable, a second beamsplitter is necessary. This beamsplitter implements another unitary rotation around an axis in the equatorial plane shifted by 90° with respect to the first beamsplitter in order to translate the longitudinal angle to a polar angle θ. The readout of the interferometer is done by detection of the population difference J_z of the two output ports, from which the relative phase φ can be deduced. The resulting sinusoidal variation of the population difference $\langle \hat{J}_z \rangle$ versus acquired relative phase φ is commonly called a *Ramsey fringe*.

Quantifying Interferometric Precision

Taking finite environmental noise into account, the sensitivity of the interferometer to small phase shifts

$$\Delta\varphi^{-1} = \left(\frac{\Delta \hat{J}_z}{\frac{\partial \langle \hat{J}_z \rangle}{\partial \varphi}} \right)^{-1} \tag{2.26}$$

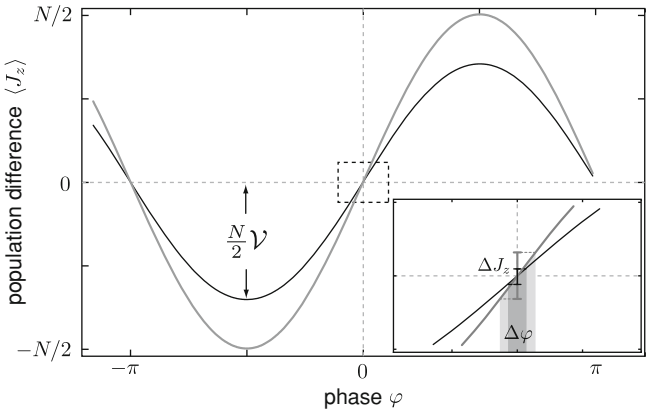

Fig. 2.7 Precision limit in Ramsey interferometry. We compare schematically the phase estimation precision in Ramsey interferometry using a coherent spin state (*gray*) and a spin squeezed state (black). The main figure shows a Ramsey fringe whose visibility $\mathcal{V}$ is maximal for a coherent spin state ($\mathcal{V} = 1$) but smaller for a spin squeezed state. Nevertheless the phase precision for a squeezed state outperforms the precision obtained for classical interferometer as shown in the zoom around the zero crossing. The projection noise is suppressed for the spin squeezed state such that the ratio of projection noise and slope of the Ramsey fringe is smaller by a factor ξ_S compared to the standard quantum limit, which explains the gain in interferometric precision

depends on the mean phase $\langle\varphi\rangle$ and is determined by the projection noise $\Delta\hat{J}_z$ and the slope of the Ramsey fringe $\partial\langle\hat{J}_z\rangle/\partial\varphi$. The point of maximum sensitivity is reached where the mean population difference is zero and the slope is maximal $(\partial\langle\hat{J}_z\rangle/\partial\varphi)_{\max} = \mathcal{V}N/2$. The visibility $\mathcal{V}$ measures the mean spin length $\langle\mathbf{J}\rangle = \mathcal{V}N/2$. Figure 2.7 illustrates the phase sensitivity of a Ramsey interferometer.

The amount of precision gain (or loss) relative to standard quantum limit is given by ξ_R^{-2} or equivalently by $\left(\xi_S^2\right)^{-1}$. The measure can be expressed in visibility $\mathcal{V}$ and spin noise in J_z direction at readout $\Delta\hat{J}_z^2$:

$$\xi_S^2 = \frac{4\Delta\hat{J}_z^2}{\mathcal{V}^2 N} \tag{2.27}$$

The absolute phase uncertainty–measured as the root mean square deviation is:

$$\Delta\varphi = \xi_S \frac{1}{\sqrt{N}} \tag{2.28}$$

Spin squeezed states feature reduced noise in one of the spin directions but excess noise in another direction can be present either due to a non-Heisenberg limited quantum state or due to an incoherent mixture of several quantum states. The former might limit precision in standard Ramsey interferometry, but specific correlated quantum states enable even enhanced interferometric precision in a generalized interferometer [33]. The latter is easily limiting interferometric precision at a level above

the standard quantum limit and experimentally it requires a large effort to prevent decoherence due to technical noise from the environment or due to finite temperature in the system. Large noise—quantum or classical—even in a spin direction that is not directly measured has a degrading effect on interferometric precision which arises due to the curved surface of the Bloch sphere. As soon as the noise amplitude is large enough such that the area of uncertainty can no longer be approximated by a plane, the mean spin is effectively shortened and the visibility decreases $\mathcal{V} < 1$.

Ramsey Interferometry with Entangled States

Entanglement can be used as a quantum resource in a Ramsey interferometric sequence in different ways. In order to increase the phase sensitivity either the slope of the signal $\partial\langle\hat{J}_z\rangle/\partial\varphi$ has to be increased or the projection noise $\Delta\hat{J}_z^2$ has to be decreased.

Slope increase can be reached by *Schrödinger cat* type entanglement which involves maximally entangled states that are very fragile to decoherence. Therefore they have been realized so far with very few particles only [34–36].

Spin squeezing aims to decrease the projection noise. This is possible in gradual steps meaning that depending on the amount of spin squeezing the precision is gradually increased. Therefore—at least for moderate levels of spin squeezing—these states are less fragile and they have been realized with a large number of particles but only with a relatively small squeezing factor [37–46]. Ramsey interferometry with spin squeezed states is schematically depicted in Fig. 2.6b where a “magic" beamsplitter produces an entangled state. Interferometric sensitivity for a coherent spin state and a spin squeezed state is compared in Fig. 2.7. For the spin squeezed state the decreased quantum fluctuations $\Delta\hat{J}_z$ reduce the projection noise while the increased fluctuations $\Delta\hat{J}_y$ cause a slight decrease of the mean spin length and therefore of the visibility of the Ramsey fringe. Nevertheless, the ratio of projection noise and slope of the Ramsey fringe—and therefore the phase sensitivity—is increased.

2.4.2 Heisenberg Limit in Quantum Metrology

The ultimate limit for metrologic precision is the *Heisenberg limit* [47], where the phase estimation error $\Delta\varphi$ is given by

$$\Delta\varphi = \frac{1}{N} \tag{2.29}$$

for N resources used in a single measurement. This fundamental limit can—up to a constant numerical factor in the order of unity—in principle be reached with both approaches mentioned above—Schrödinger cat type entanglement or spin squeezing.

Schrödinger Cats and Metrology

In the context of quantum metrology the Schrödinger cat state is frequently called a NOON state [48]. Its name originates from its form in Fock states basis:

$$|NOON\rangle = (|N, O\rangle + \mathrm{e}^{i\varphi_N}\,|O, N\rangle)/\sqrt{2} \tag{2.30}$$

It is a coherent superposition of all atoms in state $\hat{a}$ and zero atoms in state $\hat{b}$ and vice versa. In spin representation the NOON state is the superposition of the two maximal Dicke states:

$$|NOON\rangle = (|J, -J\rangle + \mathrm{e}^{i\varphi_N}\,|J, J\rangle)/\sqrt{2} \tag{2.31}$$

The increase of the signal slope for a NOON state is obvious since the phase acquired between the two components $\varphi_N = N\varphi$ is N times larger than for a coherent spin state [9, 49, 50]. Experimentally it is important to note that the readout of the interferometer can not be realized by measuring $\langle \hat{J}_z \rangle$. The reason is the vanishing mean spin length $\langle \hat{J}_x \rangle$ of this state. It has been shown that the parity of the state is a useful experimental observable to make use of NOON states in interferometry and to reach the Heisenberg limit [34, 50].

Spin Squeezed States

Spin squeezed states allow to ask for the best achievable interferometry gain demanding a finite mean spin length such that standard interferometric readout can be used.

The optimum ξ_R for a given mean spin length was found numerically in Ref. [25] and for rather small spins it is shown in Fig. 2.5. An experimental protocol to generate spin squeezed states close to the Heisenberg limit was proposed in Ref. [52].

Other Types of Quantum Correlated States

Recently it has been pointed out that the *Fisher information* is the most general criterion to measure phase sensitivity since it saturates the Quantum Cramer-Rao bound [33, 53]. Calculating the Fisher information for a coherent spin state state evolving under the non-linear Hamiltonian $\hat{H} = \chi \hat{J}_z^2$, where χ parametrizes the nonlinearity, Pezzé and Smerzi recovered Heisenberg limit like scaling for the phase precision [33]. The quantum state here is neither necessarily a NOON state nor a coherently spin squeezed state. However standard interferometric readout can not be used to extract the phase information and a new type of Bayesian readout has to be employed which was experimentally demonstrated in [53].

References

1. Kitagawa M, Ueda M (1993) Squeezed spin states. Phys Rev A 47:5138–5143
2. Wineland D, Bollinger J, Itano W, Heinzen D (1994) Squeezed atomic states and projection noise in spectroscopy. Phys Rev A 50:67–88

3. Sørensen AS, Duan L, Cirac J, Zoller P (2001) Many-particle entanglement with Bose–Einstein condensates. Nature 409:63–6
4. Metcalf H, Van der Straten P (1999) Laser cooling and trapping. Springer, New York
5. Sakurai J (1994) Modern quantum mechanics. Addison-Wesley, Reading
6. Arecchi FT, Courtens E, Gilmore R, Thomas H (1972) Atomic coherent states in quantum optics. Phys Rev A 6:2211–2237
7. Radcliffe JM (1971) Some properties of coherent spin states. J Phys A Gen Phys 4:313–323
8. Zhang W-M, Feng DH, Gilmore R (1990) Coherent states: theory and some applications. Rev Mod Phys 62:867–927
9. Giovannetti V, Lloyd S, Maccone L (2004) Quantum-enhanced measurements: beating the standard quantum limit. Science 306:1330–1336
10. Lee CT (1984) Q representation of the atomic coherent states and the origin of fluctuations in superfluorescence. Phys Rev A 30:3308–3310
11. Amico L, Fazio R, Osterloh A, Vedral V (2008) Entanglement in many-body systems. Rev Mod Phys 80:517
12. Horodecki R, Horodecki P, Horodecki M, Horodecki K (2009) Quantum entanglement. Rev Mod Phys 81:865
13. Plenio MB, Virmani S (2007) An introduction to entanglement measures. Quantum Inf Comput 7:1
14. Benatti F, Floreanini R, Marzolino U (2010) Sub-shot-noise quantum metrology with entangled identical particles. Ann Phys 325:924
15. Tóth G, Knapp C, Gühne O, Briegel HJ (2007) Optimal spin squeezing inequalities detect bound entanglement in spin models. Phys Rev Lett 99:250405
16. Tóth G, Knapp C, Gühne O, Briegel HJ (2009) Spin squeezing and entanglement. Phys Rev A 79:042334
17. Korbicz J et al (2006) Generalized spin-squeezing inequalities in N-qubit systems: theory and experiment. Phys Rev A 74:52319
18. Korbicz JK, Cirac JI, Lewenstein M (2005) Erratum spin squeezing inequalities and entanglement of N qubit states. Phys Rev Lett 95:259901
19. Korbicz JK, Cirac JI, Lewenstein M (2005) Spin squeezing inequalities and entanglement of N qubit states. Phys Rev Lett 95:120502
20. Wang X, Sanders B (2003) Spin squeezing and pairwise entanglement for symmetric multiqubit states. Phys Rev A 68:12101
21. Chaudhury S, Smith A, Anderson BE, Ghose S, Jessen PS (2009) Quantum signatures of chaos in a kicked top. Nature 461:768–771
22. Bennett CH, DiVincenzo DP, Smolin JA, Wootters WK (1996) Mixed-state entanglement and quantum error correction. Phys Rev A 54:824–3851
23. Cohen-Tannoudji C, Diu B, Laloe F (2005) Quantum mechanics. Wiley-VCH, New York
24. Ghose S, Stock R, Jessen P, Lal R, Silberfarb A (2001) Chaos, entanglement, and decoherence in the quantum kicked top. Phys Rev A 78:042318
25. Sørensen AS, Mølmer K (1949) Entanglement and extreme spin squeezing. Phys Rev Lett 86:4431–4434
26. Ramsey NF (1949) A new molecular beam resonance method. Phys Rev 76:996
27. Ramsey NF (1950) A molecular beam resonance method with separated oscillating fields. Phys Rev 78:695–699
28. Santarelli G et al (1999) Quantum projection noise in an atomic fountain: a high stability cesium frequency standard. Phys Rev Lett 82:4619–4622
29. Wasilewski W, Jensen K, Krauter H, Renema JJ, Polzik ES (2010) Quantum noise limited and entanglement assisted magnetometry. Phys Rev Lett 104:133601
30. Cronin AD, Schmiedmayer J, Pritchard DE (2009) Optics and interferometry with atoms and molecules. Rev Mod Phys 81:1051
31. Kasevich M, Chu S (1992) Measurement of the gravitational acceleration of an atom with a light-pulse atom interferometer. Appl Phys B 54:321–332

32. Gustavson TL, Bouyer P, Kasevich MA (1997) Precision rotation measurements with an atom interferometer gyroscope. Phys Rev Lett 78:2046–2049
33. Pezzé L, Smerzi A (2009) Entanglement, nonlinear dynamics, and the Heisenberg limit. Phys Rev Lett 102:100401
34. Leibfried D et al (2004) Toward Heisenberg-limited spectroscopy with multiparticle entangled states. Science 304:1476–1478
35. Roos CF, Chwalla M, Kim K, Riebe M, Blatt R (2006) 'Designer atoms' for quantum metrology. Nature 443:316
36. Nagata T, Okamoto R, O'Brien JL, Sasaki K, Takeuchi S (2007) Beating the standard quantum limit with four-entangled photons. Science 316:726–729
37. Meyer V et al (2001) Experimental demonstration of entanglement-enhanced rotation angle estimation using trapped ions. Phys Rev Lett 86:5870–5873
38. Schleier-Smith MH, Leroux ID, Vuletic V (2010) Reduced-quantum-uncertainty states of an ensemble of two-level atoms. Phys Rev Lett 104:73604
39. Leroux ID, Schleier-Smith MH, Vuletic V (2010) Implementation of cavity squeezing of a collective atomic spin. Phys Rev Lett 104:73602
40. Fernholz T et al (2008) Spin squeezing of atomic ensembles via nuclear-electronic spin entanglement. Phys Rev Lett 101:073601
41. Kuzmich A, Mandel L, Bigelow NP (2000) Generation of spin squeezing via continuous quantum nondemolition measurement. Phys Rev Lett 85:1594–1597
42. Hald J, Sørensen JL, Schori C, Polzik ES (1999) Spin squeezed atoms: a macroscopic entangled ensemble created by light. Phys Rev Lett 83:1319–1322
43. Appel J et al (2009) Mesoscopic atomic entanglement for precision measurements beyond the standard quantum limit. Proc Natl Acad Sci USA 106:10960–10965
44. Goda K et al (2008) A quantum-enhanced prototype gravitational-wave detector. Nat Phys 4:472–476
45. Vahlbruch H et al (2008) Observation of squeezed light with 10 dB quantum-noise reduction. Phys Rev Lett 100:033602
46. Estève J, Gross C, Weller A, Giovanazzi S, Oberthaler M K (2008) Squeezing and entanglement in a Bose–Einstein condensate. Nature 455:1216–1219
47. Giovannetti V, Lloyd S, Maccone L (2006) Quantum metrology. Phys Rev Lett 96:010401
48. Lee H, Kok P, Dowling J (2003) A quantum Rosetta stone for interferometry. J Mod Opt 49:2325–2338
49. Bouyer P, Kasevich MA (1997) Heisenberg-limited spectroscopy with degenerate Bose–Einstein gases. Phys Rev A 56:R1083–R1086
50. Dowling JP (1998) Correlated input-port, matter-wave interferometer: Quantum-noise limits to the atom-laser gyroscope. Phys Rev A 57:4736–4746
51. Bollinger JJ, Itano WM, Wineland DJ, Heinzen DJ (1996) Optimal frequency measurements with maximally correlated states. Phys Rev A 54:R4649–R4652
52. Pezzé L, Collins LA, Smerzi A, Berman GP, Bishop AR (2005) Sub-shotnoise phase sensitivity with a Bose–Einstein condensate Mach–Zehnder interferometer. Phys Rev A 72:043612
53. Pezzé L, Smerzi A, Khoury G, Hodelin JF, Bouwmeester D (2007) Phase detection at the quantum limit with multiphoton Mach–Zehnder interferometry. Phys Rev Lett 99:223602

http://www.springer.com/978-3-642-25636-3

Spin Squeezing and Non-linear Atom Interferometry with Bose-Einstein Condensates

Groß, C.

2012, XII, 116 p., Hardcover
ISBN: 978-3-642-25636-3